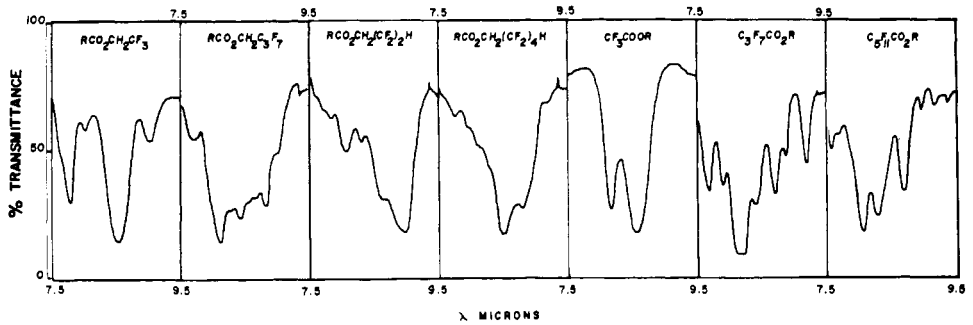

Figure 1. Characteristic infrared ← a sorption spectra

Figure 2. Catalog of characteristic absorption peaks between 700 and 100 cm.$^{-1}$ ↓

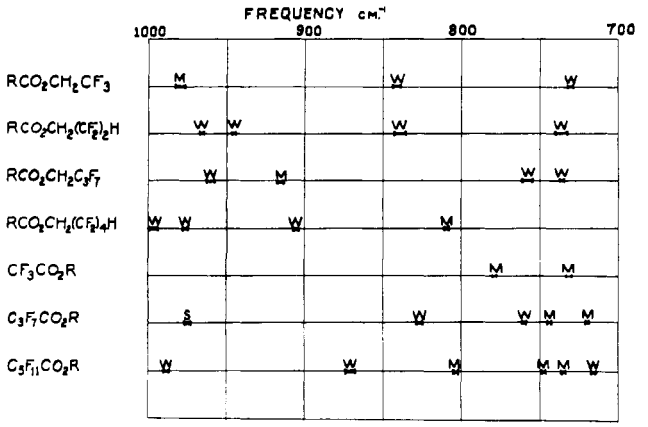

left uncovered, although less readily than the trifluoroacetates. The remaining fluorinated esters had considerably greater hydrolytic stability.

Infrared spectra showed the effect of fluorine in increasing the stretching frequency of the carbonyl (*1*) over the normal range of 1735 to 1750 cm.$^{-1}$ (5.76 to 5.71 microns). The frequency increase was larger when the fluorine was in the acyl moiety than when it was in the alkyl moiety. The observed ranges were respectively, 1790 to 1805 cm.$^{-1}$ (5.59 to 5.54 microns) and 1765 to 1780 cm.$^{-1}$ (5.67 to 5.62 microns). The smaller effect observed when fluorine was in the alkyl group reflects the insulating effect of the oxygen atom between the alkyl group and the carbonyl group.

Each series of esters derived from any single fluorinated alcohol or fluorinated acid gave a characteristic absorption profile in the range of 1050 to 1350 cm.$^{-1}$. A representative profile of each series has been duplicated in Figure 1.

In each series of compounds, characteristic absorption peaks occurred in the region of 700 to 1000 cm^{-1}. The representative peaks and relative intensities for each of the seven series of compounds are listed in Figure 2.

LITERATURE CITED

(1) Bellamy, L.J., Infra-red Spectra of Complex Molecules," pp. 182-3, Methuen, Ltd., London, 1958.
(2) Faurote, P.D., Henderson, C.M., Murphy, C.M., O'Rear, J.C., Ravner, H., *Ind. Eng. Chem.* **48**, 455 (1956).
(3) Filler, R., Fenner, J.V., Stokes, C.S., O'Brien, J.F., Hauptschein, M., *J. Am. Chem. Soc.* **75**, 2693 (1953).
(4) Filler, R., O'Brien, J.P., Fenner, J.V., Hauptschein, M., *Ibid.*, **75**, 966 (1953).
(5) Hickinbottom, W.J., "Reactions of Organic Compounds," p. 266, Longmans, Green., New York, 1948.
(6) Minnesota Mining and Manufacturing Co., "Fluorochemicals Heptafluorobutyric Acid," 1950.
(7) Newman, M.S., *J. Am. Chem. Soc.* **72**, 4783 (1950).
(8) Radell J., *Chemist Analyst* **46**, 73 (1957).
(9) Radell, J., Connolly, J.W., *J. Org. Chem.* **25**, 1202 (1960).

RECEIVED for review April 4, 1960. Accepted October 11, 1960.

Measurements of Transverse Dispersion in Granular Media

F.E. GRANE and G.H.F. GARDNER, Gulf Research & Development Co., Pittsburgh, Pa.

WHEN A HOMOGENEOUS fluid flows through a porous medium, its particles are dispersed by the combined effects of molecular diffusion and the interweaving action of the structure of the porous medium on fluid stream lines. This was observed as early as 1934 by Kitagawa (*5*). Thus, a sphere of tagged particules does not move rigidly with the average velocity of the fluid stream, but it gradually expands and mixes with the surrounding fluid. The deformation of the sphere may conveniently be resolved into a component in the direction of fluid flow and a component perpendicular to the direction of fluid flow. This paper is concerned primarily with the latter. Theoretical discussions of transverse dispersion have been given (*1, 3, 4, 6, 12, 13*) and some experimental measurements have been made at turbulent rates of flow (*1, 3*), but there are few data available (*2*) for low rates of flow at which the effects of molecular diffusion become significant. The experiments reported here were made to fill this gap.

A knowledge of the magnitude of transverse dispersion can be of importance under several circumstances. When a fluid is displaced from a porous medium by a less viscous miscible fluid, the viscous forces create an unstable pressure distribution and the less viscous fluid will penetrate the medium in the form of fingers (*9*), unless some other force field, such as gravity, has an opposing effect. These fingers are blended with the surrounding fluid by a combination of longitudinal and transverse dispersion. Hence, a quantitative measure of each is required, if the efficiency of the displacement process is to be evaluated. In general, both longitudinal and transverse dispersion are factors contributing to the motion of miscible fluids flowing in two or three dimensions.

EXPERIMENTAL PROCEDURE AND APPARATUS

The experiments performed were basically similar to those described by Bernard and Wilhelm (*1*). They investigated turbulent rates of flow and measured the steady-state distribution due to a point source in a cylindrical fluid stream. The experimental arrangement used here differs in that diffusion across a plane surface, rather than a cylindri-

cal surface, was examined. This was done to minimize mixing caused by a slight density difference in the two diffusing fluids which, at very low flow rates, might otherwise become important.

The flow chamber for the experiments was made from ⅜-inch Lucite and was 30 inches long with a rectangular cross section 1 inch wide and 2 inches high. A plain sheet of aluminum foil separated the first third of the box into two similar compartments each having a square cross section (Figure 1,*A*). Each compartment had its own inlet, so that fluids entering the chamber through them were confined by the impermeable foil and sides. Downstream from the end of the foil the two fluid streams could intermingle. A single outlet was used to carry off the effluent.

The chamber was mounted on a carriage, so that the aluminum barrier was horizontal. The carriage could be moved either horizontally by hand or vertically by an electric motor. The fluids entered the compartments at the same flow rate, each controlled by a constant rate displacement pump. For each experiment an assigned rate was maintained until a steady-state distribution of the fluids throughout the entire chamber was believed to exist.

Glass spheres of a uniform size were used to pack the box. The spheres dented the foil slightly and thus the barrier assumed a surface shape which had a negligible effect on the homogeneity of the packing. A wire screen at the outlet end kept the spheres under slight compression and prevented them from shifting.

Experiments were made with glass spheres 1.5, 0.25, and 0.074 mm. in diameter. The porosities of the packings were 37.5, 41, and 38%, respectively.

A sandstone core, cut to the same dimensions as the box and coated with epoxy resin, was also used. In this case, the aluminum divider was placed in a Lucite box, packed with 0.25-mm. glass spheres, which was aligned and abutted against one end of the sandstone core. The downstream end of the foil was 1.4 inches from the inlet face of the sandstone (Figure 1,*B*).

The distribution of fluids within the various media was measured by means of a narrow x-ray beam. This equipment was a modification of that described by Morgan, McDowell, and Doty (*7*). The x-ray tube was operated at 70 kv.p. and 2.4 ma. The beam was collimated and as it passed through the flow chamber had a cross section $\frac{1}{16} \times \frac{1}{4}$ inch and an incident strength of 50 mr. per hour. The emergent beam was detected by a ¾-inch diameter 10-stage scintillation counter (Dumont), operated at 825 volts. The thallium-activated sodium iodide crystal was mounted with Dow Corning 200 oil and covered with a 0.25-inch $\times 10^{-3}$ beryllium window and an additional screen of 0.010-inch aluminum foil placed ⅜ inch from the crystal. The counter was operated as a current integrator into a 410 micromicroammeter (Keithley). The current (10^{-7} ampere) was fed into a potentiometer balancing circuit and then led to a Speedomax 1-mv. recorder (Leeds and Northup) with a chart speed of 3 inches per minute.

One fluid used was Soltrol C. (Phillips Petroleum Co.), of density 0.751 gram per cc., and viscosity 1.384 centipoises at 24.2° C. The other fluid, in most cases, was Soltrol C containing 5% of 1-iodopentane (Eastman Kodak) of density 0.789 gram per cc., and viscosity 1.328 centipoises at 24.2° C. Some experiments were also made with solutions containing 10, 5, 2.5, and 1.1% of 1-iodopentane to test the effect of density difference. The intensity of the emergent x-ray beam depends on absorption by Lucite, glass, Soltrol, and 1-iodopentane. Calibration curves were obtained by saturating the media with solutions of known strength. Hence, chart readings could be converted directly to concentrations of 1-iodopentane in Soltrol. The denser fluid was pumped into the lower compartment. This ensured a stable, two-dimensional equilibrium distribution. The carriage was placed at a selected distance from the end of the aluminum barrier and then driven vertically so that the x-ray beam scanned a vertical section of the core. This record was converted to a concentration-distance profile for that section. In general, a steady-state distribution was attained after several pore volumes of fluid had passed through the chamber. This was checked by approaching the steady state from opposite directions. Thus, when the fluid flow was stopped, molecular diffusion gradually mixed the fluids and the concentration gradient was slowly decreased. On resumption of the original flow rate, the steady-state profile was approached through gradually increasing gradients. On the other hand, the concentration gradient could be increased by raising the flow rate. On resuming the original rate of flow, equilibrium was approached through gradually decreasing gradients. If the gradient attained through increasing gradients was the same as the gradient attained through decreasing gradients, it was assumed to be the true steady-state value.

The coefficient of transverse dispersion was calculated from the measured concentration gradient at 50% concentration and at a distance of 20 cm. from the end of the aluminum barrier, by using Equation 6.

To test the validity of Equation 6, profiles were measured at various distances. According to theory, the concentration gradient at 50% concentration should vary as the reciprocal of the square root of the distance from the downstream edge of the foil. This was confirmed for the 0.025-cm. spheres and the consolidated sandstone.

THEORY

All the theoretical discussions (*1, 3, 4, 6, 12, 13*) of dispersion in a homogeneous fluid agree that after sufficient time, the distribution of particles is gaussian. Thus, an initial sphere of tagged particles gradually expands and eventually resembles a prolate spheroid with major axis lying in the direction of flow. At sufficiently low flow rates, molecular diffusion is dominant and the prolate spheroid is almost spherical; the original particles and the surrounding fluid having become irreversibly mixed. At sufficiently high flow rates, the effect of molecular diffusion is negligible and the spreading of the sphere is caused by the interweaving of streamlines. In the limit of no molecular diffusion, the tagged particles and the surrounding fluid form a syzygy and its prolate shape reflects the geometrical structure of the porous medium. At intermediate rates, both microscopic and macroscopic mixing contribute to dispersion.

For steady-state two-dimensional flow in the x-direction the diffusion-convection equation may be written (*11*)

$$V \frac{\partial S}{\partial X} = E_L \frac{\partial^2 S}{\partial X^2} + E_T \frac{\partial^2 S}{\partial y^2} \qquad (1)$$

where S is the concentration of the diffusing material, V is the average fluid particle velocity, and E_L and E_T are coefficients of effective dispersion in the direction of flow and at right angles, respectively. These coefficients depend on the structure of the porous medium, the rate of fluid flow, and the coefficient of self-diffusion of the fluid. The experimental results obtained may be interpreted conveniently as giving the dependence of E_T on V for two types of porous media.

An exact solution of Equation 1 is easily obtained which corresponds to the experimental flow pattern with idealized boundary conditions. The upper and lower boundaries are supposed infinitely distant from the divider which, itself, is supposed infinitely long. A correction may be made for the presence of boundaries at a finite distance, but this is negligible at all flow rates used and, hence, the idealized solution is sufficiently accurate.

The solution may be constructed by introducing parabolic

coordinates with the origin at the downstream end of the divider and the x-axis in the direction of flow. The transformation to parabolic coordinates is defined by the equations

$$2Vx = E_L(\eta^2 - \zeta^2)$$

$$Vy = (E_L E_T)^{1/2}\zeta\eta \tag{2}$$

Equation 1 then becomes

$$\frac{\partial^2 S}{\partial \zeta^2} + \frac{\partial^2 S}{\partial \eta^2} + \zeta \frac{\partial S}{\partial \zeta} - \eta \frac{\partial S}{\partial \eta} = 0 \tag{3}$$

Assuming that S is independent of η, this equation reduces to an ordinary differential equation for which a solution is

$$S = \tfrac{1}{2}\,[1 - erf\ \zeta/(2)^{1/2}] \tag{4}$$

The arbitrary constants which arise on integration have been chosen so that Equation 4 satisfies the required boundary conditions. Thus, along the negative x-axis, which is defined in parabolic coordinates by $\eta = 0$, the gradient $\partial S/\partial y$ obviously vanishes; physically this corresponds to the presence of an impermeable barrier. Below the barrier and close to the inlet, where $\eta \to 0$ and $\zeta \to -\infty$, the value of S given by Equation 4 approaches unity. This corresponds physically to the injection of tracer material into the lower compartment. On the other hand, above the barrier and close to the inlet where $\eta \to 0$ and $\zeta \to \infty$ the value of S approaches zero. Thus, the fluid entering the upper compartment contains no tracer fluid.

A simple way of picturing this solution is to draw the curves on which S is constant. Evidently, they are parabolas with foci at the end of the barrier and axes in the direction of flow. The equation of the curve along which $S = 0.25$ above the x-axis and $S = 0.75$ below the x-axis is

$$y^2 = \frac{0.91\,E_T}{V}\,x + \frac{0.2\,E_T E_L}{V^2} \tag{5}$$

Along the positive x-axis, the concentration is 0.5 at all points. The concentration gradient for a vertical scan at these points is easily obtained from Equation 4 and gives

$$\left(\frac{\partial S}{\partial y}\right)_{y=0} = \frac{1}{(4\pi\,E_T x/V)^{1/2}} \tag{6}$$

EXPERIMENTAL RESULTS

The values of E_T, calculated from the observed concentration gradients by means of Equation 6, are listed in Table I for the three packings of spheres used. Since each packing has a porosity of about 40%, it seems reasonable to assume that they are homologous. If they are homologous and if mixing is caused solely by molecular diffusion and the geometrical structure of the packings, then a plot of the dimensionless Peclet number $d_p V/E_T$ *vs.* the dimensionless group $d_p V/D_0$ should give the same curve for all particle sizes. The data are plotted in this form in Figure 2. The points for the smaller particle sizes virtually lie on the same curve, but results for the largest spheres are seriously at variance. In fact, only two points fit within the range of the graph shown, the remainder being about three times larger than might be expected. This suggests that the density difference decreases the amount of mixing when permeability is large. A series of experiments was made to test this hypothesis.

At a fixed velocity of 0.02 cm. per second, measurements were made with the 0.15-cm. diameter spheres at concentrations of 10, 5, 2.5, and 1.1% of the tracer 1-iodopentane in the flowing oil. The corresponding values of $d_p V/E_T$ are plotted against the density difference between the fluids (Figure 3). Extrapolation of these data to 0% of the tracer suggests a limiting value of about 22. This limiting value, indicated in Figure 2 by the arrow and dotted square, lies on the curve suggested by the smaller sized packing. It was concluded that the homologous packings did, in fact, lead to a unique curve, provided the density difference between the fluids was not large.

The data for a series of experiments performed with the Berea sandstone core are given in Table II.

Table I. Transverse Dispersion Table

V, Cm./Sec.	$d_p = 0.025$ Cm. $E_T \times 10^6$ Sq. Cm./Sec.	$d_p = 0.0074$ Cm. $E_T \times 10^6$ Sq. Cm./Sec.	$d_p = 0.15$ Cm. $E_T \times 10^6$ Sq. Cm./Sec.
0.4	406	...	...
0.1	127	60	170
0.05	66	40	110
0.02	36	23	61
0.01	30	...	...
0.004	17	8.8	17
0.002	12	...	...
0.0008	9.6	8.0	4.8
0.00016	9.4	...	8.0

DISCUSSION OF EXPERIMENTAL RESULTS

The consistency of the measurements for the three packings of spherical particles attests to their validity. An auxiliary measurement of the static dispersion coefficient—i.e., $V = 0$—was also made in a 3-inch i.d. vertical cylinder, packed with glass spheres to a porosity of about 40%. Soltrol was displaced from the cylinder by tagged Soltrol, so that the interface was horizontal and near the center of the cylinder. By observing the concentration profiles at periods of 24 hours for 4 days, a value of 8.3×10^{-6} sq. cm. per second was calculated for E_T. This is slightly smaller than the value measured in the flow chamber at the lowest rate.

The coefficient E_T must be multiplied by the porosity in order to obtain the coefficient of static diffusion D in a porous medium, as this is usually defined. Thus,

$$D = \phi\,E_T \tag{7}$$

The ratio of D to D_0, the coefficient of diffusion in the absence of the porous medium, is well known for packings of spherical particles. Penman (*8*) concluded that $D/D_0 = 0.66\,\phi$. However, the extensive data of Wyllie and Gregory (*14*) for the formation resistivity factor of packings of spheres suggest that $D/D_0 = \tfrac{1}{2}\phi + \tfrac{1}{2}\phi^2$ is a better empirical result. Assuming $\phi = 0.4$ it follows that D_0 for 1-iodopentane in Soltrol is about 1.2×10^{-5} sq. cm. per second.

Bernard and Wilhelm (*1*) measured the Peclet number for spherical particles at turbulent rates of flow and some of their data are shown in Figure 2. Theoretical calculations by Latinen (*6*) led to a value of about 11 for the Peclet number, if flow was fully turbulent and complete mixing could be assumed when the fluids from two pores met. With increased correlation between streamlines—i.e., less turbulence—the Peclet number should be greater.

Table II. Transverse Dispersion in Sandstone

V, Cm./Sec.	E_T/V, Cm.	V, Cm./Sec.	E_T/V, Cm.
0.00183	0.0060	0.0134	0.0039
0.00268	0.0051	0.0268	0.0037
0.00535	0.0044	0.0670	0.0037

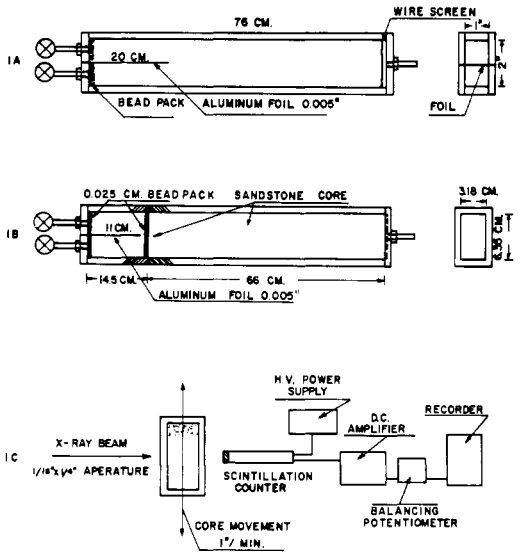

Figure 1. Schematic diagram of apparatus

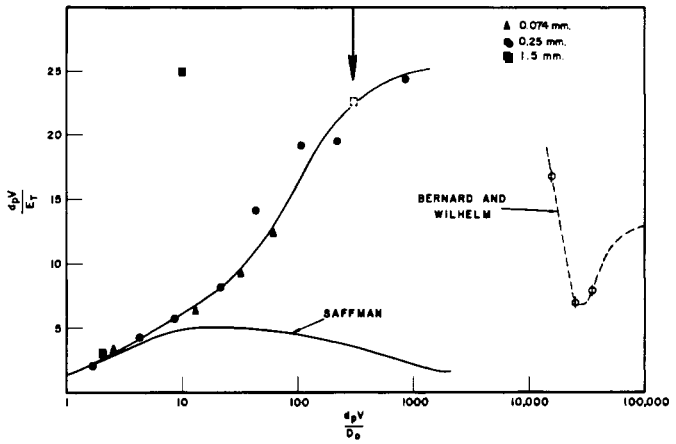

Figure 2. Effect of density difference on Peclet number for spheres 1.5 mm. in diameter at a fixed flow rate

At low rates of flow, the Peclet number should again be small, because molecular diffusion then causes a large amount of mixing. Hence there is probably a value of $V\,d_p/D_0$ at which the Peclet number is a maximum. An indication of this is shown by the data plotted in Figure 2.

A statistical model of a porous medium, considered as an assemblage of randomly oriented, equally straight, circular capillary tubes, was investigated by Josselin de Jong (*3*) and analyzed more completely by Saffman (*12, 13*). The theoretical curve for the Peclet number, according to this theory, assumes that the length of each capillary tube is equal to the diameter of each particle (Figure 2). The agreement with data is not good and while it may be improved somewhat by assuming a shorter pore length, there seems to be a more basic reason for the disagreement. A packing of spherical particles has an open pore structure compared with the capillary model, and a streamline through the packing does not point in any direction with equal probability, but is correlated with the average direction of flow. Thus, a basic assumption of the theory seems unrealistic for packings of spherical particles. The data support this view, as the amount of transverse dispersion is very small at high flow rates.

The pore space of the Berea sample may provide a closer physical realization of the model than that of the packings because of the cementing material it contains. This would be true if the cement was concentrated at the grain to grain contacts. For the sandstone used, the average grain diameter was about 180 microns. The average pore neck radius, calculated from the pressure required to fill half-full with mercury an evacuated sample of the rock, was 15 microns.

According to the theory of the capillary model, the value of D/D_0 is equal to $\phi/3$. Experimental data on sandstones suggest that D/D_0 is equal to about $1.4\phi^2$. By coincidence, these values are equal at about $\phi = 0.2$, which is close to the porosity of the sandstone used in the experiments. To check on this coincidence, a plug was cut from the sandstone in the direction perpendicular to the plane of the barrier, and D/D_0 was measured by the usual procedure (*14*) for measuring formation resistivity factors. This value of D/D_0 was 0.068; the value from the capillary model is 0.072.

The mechanism of transverse dispersion at high flow rates is dominated by the structure or grain size of the porous medium and influenced only slightly, if at all, by molecular diffusion. Estimates of the dispersion to be expected (*3, 6, 12*) give E_T/V equal to $\frac{3}{16}$ times the length of each capillary tube. The measured value of E_T/V at high flow rates was about 0.0037. Hence, to obtain agreement with this result, the length of the equivalent capillary tube of the model would have to be 197 microns. This is about the same size as the average diameter of the sandstone grain, which was 180 microns.

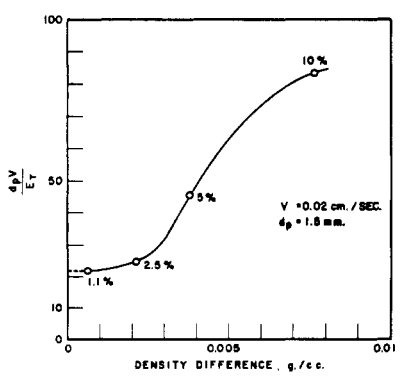

Figure 3. Peclet number for packing of spherical particles

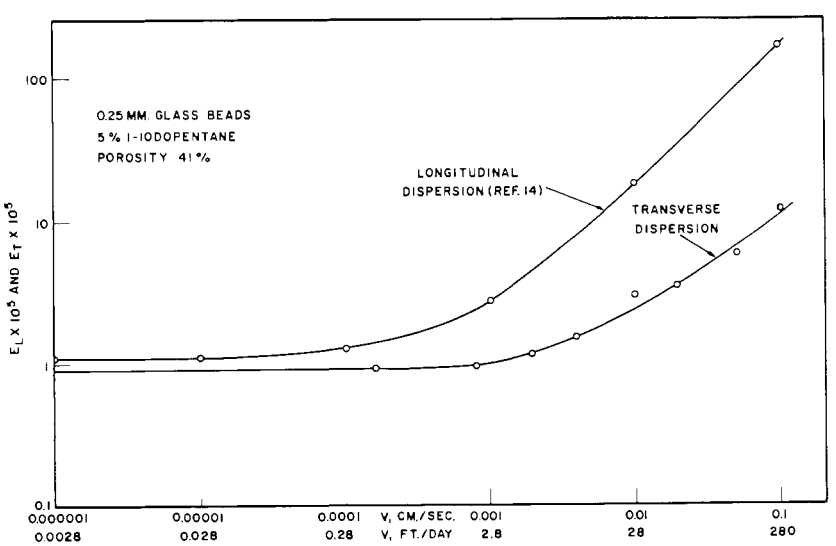

Figure 4. Plot of longitudinal and transverse coefficients of dispersion vs. velocity →

It is thus possible to demonstrate some quantitative agreement between the theory of the capillary model and the measured behavior of the sandstone. However, the agreement is certainly fortuitous at low flow rates, where the actual variation of D/D_0 with porosity is well known and different from theory.

LONGITUDINAL DISPERSION

The flow system and experiments described here are not suitable for measuring longitudinal dispersion. However, experiments have been performed to measure longitudinal dispersion in situ (*10*) by use of radioactive tracers, for both packings of glass spheres and a Berea sandstone similar to the one used for the measurement of lateral dispersion. A comparison of longitudinal and transverse dispersion is therefore possible.

The coefficients of longitudinal and transverse dispersion are plotted as a function of the average fluid velocity for a packing of 0.25-mm. spheres (Figure 4) and for sandstone (Figure 5). At high flow rates in both cases, the latter is much less than the former. This difference is in the same direction as statistical theory (*4*) indicates, but the observed ratio of the coefficients is much larger than the calculated ratio. This discrepancy, in the case of sandstone, may be due to the effect of pore size distribution. Lateral dispersion, which is primarily due to the average width of the particles, will not be increased greatly by the presence of fine pores, but longitudinal dispersion, which primarily depends on average velocity within each pore, is very sensitive to the existence of fine pores or dead end spaces.

For some practical applications the variation of E_T with V is negligible. Thus, flow rates in oil reservoirs are typically less than 1 foot per day and this is below the velocity at which E_T becomes velocity-dependent in the Berea sandstone. If this is typical of all oil-bearing rocks, then within the range of reservoir rates the transverse coefficient E_T may be assumed constant, whereas the longitudinal coefficient E_L is proportional to velocity.

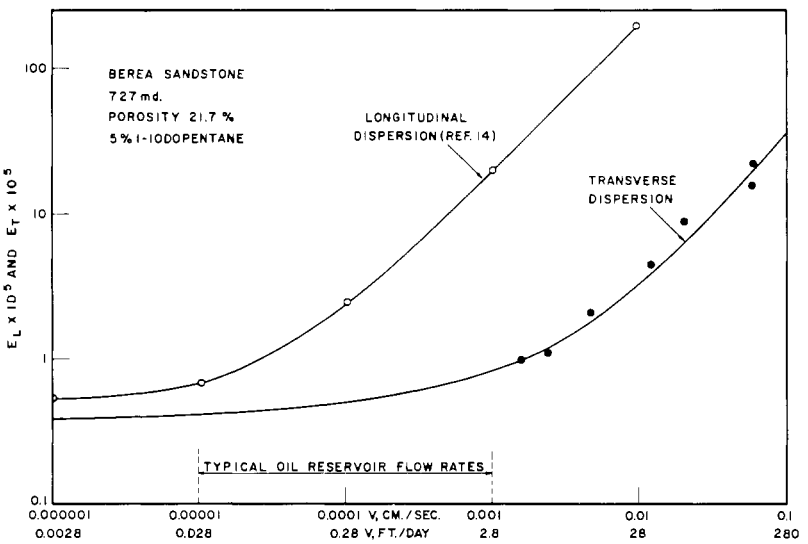

Figure 5. Coefficients of longitudinal and transverse dispersion for a sandstone at various flow rates

CONCLUSIONS

At sufficiently low flow rates transverse and longitudinal dispersion are equal and are determined by the coefficient of molecular diffusion of the fluid and the formation factor of the porous medium. At sufficiently high flow rates in consolidated media transverse and longitudinal dispersion are proportional to the velocity of flow and independent of fluid properties. Transverse dispersion may be less than longitudinal dispersion by a factor of 50. In packings of glass spheres, the coefficient of transverse dispersion appeared to increase less rapidly than the first power of the flow rate at high flow rates. At flow rates which are usual in oil reservoirs, transverse dispersion is independent of flow rate, whereas longitudinal dispersion increases significantly with flow rate in the same range.

NOMENCLATURE

- V = average fluid particle velocity, cm./sec.
- D_0 = coefficient of diffusion in free liquid, sq. cm./sec.
- D = coefficient of diffusion in liquid confined by the porous medium, sq. cm./sec.
- E_T = coefficient of transverse dispersion, sq. cm./sec.
- E_L = coefficient of longitudinal dispersion, sq. cm./sec.
- S = concentration of tracer
- d_p = particle diameter, cm.

ACKNOWLEDGMENT

The physical Science Division of Gulf Research & Development Co. designed and maintained the scintillation counter and amplifiers used.

LITERATURE CITED

(1) Bernard, R.A., Wilhelm, R.H., *Chem. Eng. Progr.* **46**, 233–44 (1950).
(2) Blackwell, R.J., A.I.Ch.E.-Soc. Petrol. Engrs. Symposium Preprint **29** (1959).
(3) Dorweiler, V.P., Fahien, R.W., *A.I.Ch.E. Journal* **5**, 139–44 (1959).
(4) Josselin de Jong, G. de, *Trans. Am. Geophys. Union* **39**, 67–74 (1958).
(5) Kitagawa, K., *Kyoto Imp. Univ., Mem. Coll. Sci., Ser. A* **17**, 37–42, 431–41 (1934).
(6) Latinen, G.A., Ph. D. thesis, Princeton University, Princeton, N. J., 1954.
(7) Morgan, F., McDowell, J.M., Doty, E.C., *Trans. AIME* **189**, 183–94 (1950).
(8) Penman, H.L., *J. Agr. Sci.* **30**, 438 (1940).
(9) Perrine, R.L., A.I.Ch.E.-Soc. Petrol. Engrs. Symposium Preprint **42** (1959).
(10) Raimondi, P., Gardner, G.H.F., Petrick, C.B., *Ibid.*, **43**.
(11) Roberts, O.F.T., *Proc. Royal Soc., Ser. A.* **1923**, 104.
(12) Saffman, P.G., *J. Fluid Mech.* **6**, 321–49 (1959).
(13) *Ibid.*, **7**, 194–208 (1960).
(14) Wyllie, M.R.J., Gregory, A.R., *Trans. AIME* **198**, 103 (1953).

RECEIVED for review April 25, 1960. Accepted August 10, 1960.